Biogeosciences, 13, 323–340, 2016
www.biogeosciences.net/13/323/2016/
doi:10.5194/bg-13-323-2016
© Author(s) 2016. CC Attribution 3.0 License.

Biogeosciences

Isotopic evidence for biogenic molecular hydrogen production in the Atlantic Ocean

S. Walter[1,a], **A. Kock**[2], **T. Steinhoff**[2], **B. Fiedler**[2], **P. Fietzek**[2,5], **J. Kaiser**[3], **M. Krol**[1], **M. E. Popa**[1], **Q. Chen**[4], **T. Tanhua**[2], **and T. Röckmann**[1]

[1]Institute for Marine and Atmospheric Research (IMAU), Utrecht University, the Netherlands
[2]Marine Biogeochemistry, GEOMAR/Helmholtz-Centre for Ocean Research, Kiel, Germany
[3]Centre for Ocean and Atmospheric Sciences, School of Environmental Sciences, University of East Anglia, Norwich, NR4 7TJ, UK
[4]Department of Atmospheric Sciences, University of Washington, Seattle, Washington, USA
[5]Kongsberg Maritime Contros GmbH, Kiel, Germany
[a]now at: Energy research Center of the Netherlands (ECN), Petten, the Netherlands

Correspondence to: S. Walter (s.walter@uu.nl)

Received: 14 September 2015 – Published in Biogeosciences Discuss.: 8 October 2015
Revised: 20 December 2015 – Accepted: 27 December 2015 – Published: 15 January 2016

Abstract. Oceans are a net source of molecular hydrogen (H_2) to the atmosphere. The production of marine H_2 is assumed to be mainly biological by N_2 fixation, but photochemical pathways are also discussed. We present measurements of mole fraction and isotopic composition of dissolved and atmospheric H_2 from the southern and northern Atlantic between 2008 and 2010. In total almost 400 samples were taken during 5 cruises along a transect between Punta Arenas (Chile) and Bremerhaven (Germany), as well as at the coast of Mauritania.

The isotopic source signatures of dissolved H_2 extracted from surface water are highly deuterium-depleted and correlate negatively with temperature, showing δD values of (-629 ± 54) ‰ for water temperatures at (27 ± 3) °C and (-249 ± 88) ‰ below (19 ± 1) °C. The results for warmer water masses are consistent with the biological production of H_2. This is the first time that marine H_2 excess has been directly attributed to biological production by isotope measurements. However, the isotope values obtained in the colder water masses indicate that beside possible biological production, a significant different source should be considered.

The atmospheric measurements show distinct differences between both hemispheres as well as between seasons. Results from the global chemistry transport model TM5 reproduce the measured H_2 mole fractions and isotopic composition well. The climatological global oceanic emissions from the GEMS database are in line with our data and previously published flux calculations. The good agreement between measurements and model results demonstrates that both the magnitude and the isotopic signature of the main components of the marine H_2 cycle are in general adequately represented in current atmospheric models despite a proposed source different from biological production or a substantial underestimation of nitrogen fixation by several authors.

1 Introduction

Molecular hydrogen (H_2) is the second most abundant reduced compound in the atmosphere after methane (CH_4). H_2 is not a radiatively active gas itself, but – via its role in atmospheric chemistry – it indirectly influences the lifetime of the greenhouse gas CH_4 and several air pollutants (Prather, 2003; Schultz et al., 2003; Tromp et al., 2003; Warwick et al., 2004; Jacobson, 2005, 2008; Feck et al., 2008; Ehhalt and Rohrer, 2009; Popa et al., 2015). The main H_2 sources are photo-oxidation of CH_4 and non-methane volatile organic compounds (NMVOCs) in the atmosphere and combustion processes at the surface, whereas soil deposition and oxidation by hydroxyl radicals ($HO^\bullet$) are the main sinks. Oceans are a minor but significant source to the global H_2 budget with a mean estimated contribution of 7 %. However, estimates of the oceanic contribution range from 1 to 15 % in different studies, indicating high uncertainties (Novelli et al., 1999; Hauglustaine and Ehhalt, 2002; Ehhalt and Rohrer, 2009; Pieterse et al., 2013 and references herein,).

Oceanic H_2 production is assumed to be mainly biological, as a by-product of nitrogen (N_2) fixation (e.g., Conrad, 1988; Conrad and Seiler, 1988; Moore et al., 2009, 2014). H_2 is produced during N_2 fixation in equimolar proportions, but also reused as an energy source. The H_2 net production rate during N_2 fixation depends on environmental conditions and also on microbial species (Bothe et al., 1980, 2010; Tamagnini et al., 2007; Wilson et al. 2010a). Besides N_2 fixation, abiotic photochemical production from chromophoric dissolved organic matter (CDOM) and small organic compounds such as acetaldehyde or syringic acid has also been found to be a source of hydrogen in the oceans (Punshon and Moore, 2008a, and references therein).

Unfortunately, measurements that constrain the temporal and spatial patterns of oceanic H_2 emissions to the atmosphere are sparse. Vertical profiles display highest concentrations in the surface layer (up to $3\,\mathrm{nmol\,L^{-1}}$) and a sharp decrease with depth towards undersaturation, where the reasons for the undersaturation are not fully understood yet (e.g., Herr et al., 1981; Scranton et al., 1982; Conrad and Seiler, 1988). Tropical and subtropical surface waters are supersaturated up to 10 times or even more with respect to atmospheric H_2 equilibrium concentrations, and therefore a source of H_2 to the atmosphere. This is in contrast to temperate and polar surface waters, which are generally undersaturated in H_2 (Scranton et al., 1982; Herr et al., 1981, 1984; Herr, 1984; Conrad and Seiler, 1988; Seiler and Schmidt, 1974; Lilley et al. 1982; Punshon et al., 2007; Moore et al., 2014).

Additional information to constrain the global H_2 budget and to gain insight into production pathways comes from the analysis of the H_2 isotopic composition (quantitatively expressed as isotope delta value, δD, see Sect. 2.2). Different sources produce H_2 with characteristic δD values. Moreover, the kinetic isotope fractionation in the two main removal processes, soil deposition and reaction with $HO^{\bullet}$, is different. The combined action of sources and sinks leads to tropospheric H_2 with a δD of +130 ‰ relative to Vienna Standard Mean Ocean water (VSMOW), (Gerst and Quay, 2001; Rhee et al., 2006; Rice et al., 2010; Batenburg et al., 2011). In sharp contrast, surface emissions of H_2 from fossil fuel combustion and biomass burning have δD values of approximately −200 and −300 ‰, respectively (Gerst and Quay, 2001; Rahn et al., 2002; Röckmann et al., 2010a; Vollmer et al., 2010). As originally proposed by Gerst and Quay (2001), isotopic budget calculations require the photochemical sources of H_2 to be enriched in deuterium, with δD values between +100 and +200 ‰ (Rahn et al., 2003; Röckmann et al., 2003; Feilberg et al., 2007; Nilsson et al., 2007, 2010; Pieterse et al., 2009; Röckmann et al., 2010b). Biologically produced H_2 has the most exceptional isotopic composition with δD of approximately −700 ‰ (Walter et al., 2012), reflecting strong preference of biogenic sources for the lighter isotope ^{1}H.

The aim of the study was (I) to determine the δD of dissolved H_2 and gain more information about possible sources, and (II) to get a high-resolution picture of the distribution of atmospheric H_2 along meridional Atlantic transects during different seasons and compare it with global model results. Samples were taken on four cruises along meridional Atlantic transects in the Southern Hemisphere and the Northern Hemisphere and on one cruise at the coast of Mauritania. A total of almost 400 atmospheric and 22 ocean surface water samples were taken, covering two seasons between 2008 and 2010.

2 Methods

2.1 Cruise tracks

During four cruises of RV *Polarstern* and one of RV *L'Atalante* between February 2008 and May 2010, air and seawater samples were collected (see Fig. 1, Table 1). The cruises of RV *Polarstern* were part of the OceaNET project (autonomous measuring platforms for the regulation of substances and energy exchange between ocean and atmosphere, Hanschmann et al., 2012).

They covered both hemispheres, between Punta Arenas (Chile, 53° S/71° W) and Bremerhaven (Germany, 53° N/8° E). South–north transects were carried out in boreal spring (April/May) and north–south transects in boreal autumn (October/November). The transects followed similar tracks as the Atlantic Meridional Transect (AMT) programme (http://amt-uk.org/) and crossed a wide range of ecosystems and oceanic regimes, from sub–polar to tropical and from euphotic shelf seas and upwelling systems to oligotrophic mid–ocean gyres (Robinson et al., 2009; Longhurst, 1998).

The RV *L'Atalante* followed a cruise track from Dakar (Senegal) to Mindelo (Cape Verde), covering a sampling area along the coast of Mauritania and a transect to the Cape Verde Islands. This area is characterized by strongly differing hydrographical and biological properties with an intensive seasonal upwelling. Area and cruise track are described in more detail in Walter et al. (2013) and Kock et al. (2008).

2.2 Atmospheric air sampling

Discrete atmospheric air samples were taken on-board RV *Polarstern* at the bridge deck, using 1 L borosilicate glass flasks coated with black shrink-hose (NORMAG), with 2 Kel-F (PCTFE) O-ring sealed valves. The flasks were preconditioned by flushing with N_2 at 50 °C for at least 12 h; the N_2 remained in the flask at ambient pressure until the sampling. During sampling the flasks were flushed for 4 min with ambient air at a flow rate of $12\,\mathrm{L\ min^{-1}}$ using Teflon tubes and a membrane pump (KNF VERDER PM22874-

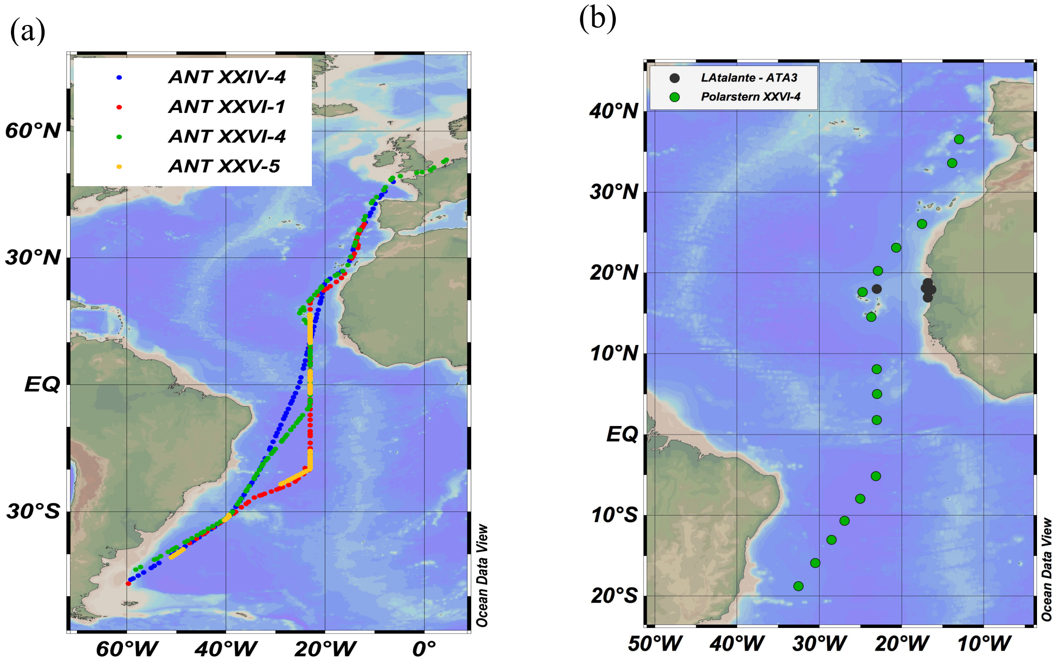

Figure 1. (a) cruise tracks of the RV *Polarstern*, dots indicate positions of discrete atmospheric air sampling, **(b)** positions of surface water headspace sampling during ANT-XXVI/4 ($n = 16$, green dots) and the RV *L'Atalante* ATA-3 cruise ($n = 6$, black dots).

Table 1. Overview of sample distribution during the cruises: type A are discrete atmospheric samples, type H are headspace samples extracted from the surface water. The sample numbers in brackets give the number of measured samples in the Northern Hemisphere (NH) and Southern Hemisphere (SH).

Cruise	Date	Position (start–end)	Nr. of Samples (NH/SH)	Type
ANT-XXIV/4	18.04.–20.05.2008	59.15° W/46.13° S–06.21° W / 47.96° N	95 (44 NH/51 SH)	A
ANT-XXV/5	11.04.–24.05.2009	50.99° W/40.82° S–23.05° W/16.55° N	91 (30 NH/61 SH)	A
ANT XXVI/1	16.10.–25.11.2009	12.05° W/37.96° N–47.28° W/37.43° S	60 (29 NH/31 SH)	A
ANT XXVI/4	07.04.–17.05.2010	58.14° W/43.75° S–04.46° E/53.15° N	114 (56 NH/58 SH)	A
ANT XXVI/4	07.04.–17.05.2010	32.53° W/18.79° S–13.00° W/36.54° N	16 (10 NH/6 SH)	H
L'Atalante ATA-3	03.02.–20.02.2008	17.83° N/16.56° W–17.60° N/24.24° W	6 (6N H/0 SH)	H

86 N86ANDC). The sample air was dried with Drierite$^{\circledR}$ ($CaSO_4$). The flasks were finally pressurized to approximately 1.7 bar, which allows duplicate measurements of the H_2 isotopic composition of an air sample.

Table 1 gives an overview of the sampling scheme for discrete H_2 samples. In total 360 samples were collected, regularly distributed over the transects at 4 to 6 h intervals. In 2009 the resolution of sampling was enhanced to one sample per 2 h and focused on five sub-sections of the transect, in an attempt to resolve dial variability.

Samples were always taken at the downwind side of the ship to exclude a possible contamination by ship diesel exhaust. One atmospheric sample was taken directly inside the ship's funnel of RV *Polarstern* to determine the mole fraction and δD of ship diesel exhaust as a possible contamination source. This first measurements for ship diesel exhaust gave an H_2 mole fraction of (930.6 ± 3.2) nmol mol^{-1} and a δD of (-228.6 ± 5.0) ‰. In the following, we will use the abbreviation "ppb" $= 10^{-9}$ in place of the SI unit "nmol mol^{-1}".

2.3 Headspace sampling from surface waters

In addition to the atmospheric air samples, 16 headspace samples from surface water were taken during the RV *Polarstern* cruise ANT-XXVI/4 in April/May 2010 and 6 samples during the RV *L'Atalante* cruise in February 2008. The experimental setup (Fig. 2) was a prototype, and deployed for the first time to extract headspace air from surface water for isotopic composition measurements of molecular H_2. It consists of a glass vessel (10 L) and an evacuation/headspace sampling unit.

The glass vessel was evacuated for at least 24 h before sampling, using a Pfeiffer vacuum DUO 2.5A pump, with a capacity of 40 L min^{-1} (STP: 20 °C and 1 bar). Water sam-

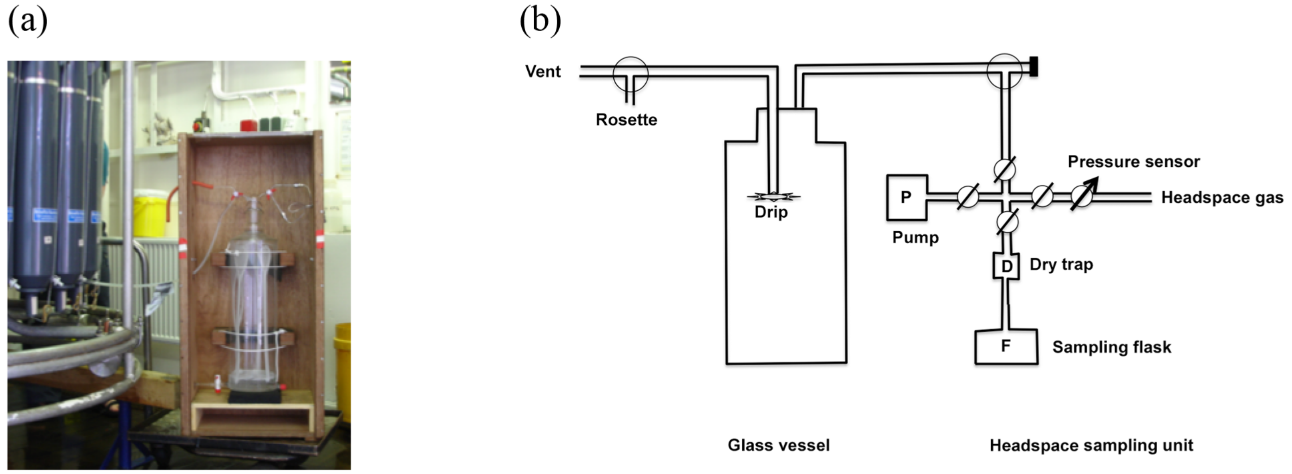

Figure 2. Experimental setup for headspace sampling, **(a)** sampling of the surface water into the glass vessel, connected to the Niskin bottle rosette, **(b)** scheme of the experimental setup.

ples were taken from 5 m depth (RV *Polarstern* cruises) or 10 m depth (RV *L'Atalante* cruise) using a 24-Niskin-bottle rosette with a volume of 12 L each. Sampling started immediately after return of the bottle rosette on-board and from a bottle dedicated to the H_2 measurements. The evacuated glass vessel was connected to the Niskin bottle by Teflon tubing, which was first rinsed with approximately 1 L surface water. Then, 8.4 L water streamed into the evacuated flask (Fig. 2), using a drip to enhance the dispersion of the sample water. After connection of the headspace-sampling unit, the lines were first evacuated and then flushed with a makeup gas several times. During the RV *L'Atalante* cruise a synthetic air mixture with an H_2 mixing ratio below threshold was used as makeup gas. The makeup gas used during the RV *Polarstern* cruises was a synthetic air mixture with an H_2 mole fraction of (543.9 ± 0.3) ppb and a δD of (93.1 ± 0.2) ‰. The mole fraction of the makeup gas was determined by the Max Planck Institute for Biogeochemistry and is given on the MPI2009 scale (Jordan and Steinberg, 2011). The glass vessel was pressurized to approximately 1.7 bar absolute with the makeup gas and the total headspace (added makeup gas plus extracted gas from the water sample) was then flushed to a pre-evacuated sample flask. The flasks were of the same type as for the atmospheric sampling: 1 L borosilicate glass flasks (NORMAG), coated with black shrink-hose to minimize photochemical reactions inside and sealed with 2 Kel-F (PCTFE) O-ring sealed valves. All flasks were previously conditioned by flushing with N_2 at 50 °C for at least 12 h and evacuated for at least 12 h directly before use. The whole sampling procedure took around 15 min: (4.0 ± 0.5) min flushing surface water to the evacuated glass vessel, (8.0 ± 1.0) min to connect the glass vessel to the sampling unit and evacuate the lines, and (3.0 ± 0.5) min to add and pressurize the glass vessel with the makeup gas and take the headspace sample. The surface water temperature was on average (0.9 ± 0.6) °C higher than the air temperature. Given that most of the apparatus was at air temperature and that the headspace will adjust to ambient temperature relatively quickly during equilibration the air temperature was used for calculations. Since the temperature dependence of H_2 solubility is less than 0.3 % per K for seawater between 16 and 30 °C (as encountered here) and view of the large H_2 saturations (see below), the error associated with this assumption is negligible. Flasks were stored in the dark until measurement. Additionally, atmospheric samples were taken at the same location of headspace sampling (Table 4).

2.4 Measurements

2.4.1 Atmospheric H_2 and δD (H_2) in discrete samples

The mole fraction and isotopic composition of molecular H_2 was determined using the experimental setup developed by Rhee et al. (2004) and described in detail in Walter et al. (2012, 2013) and Batenburg et al. (2011). The D / ^{1}H molar ratio in a sample, R_{sample}(D / H), is quantified as the relative deviation from the D / ^{1}H molar ratio in a standard, R_{standard}(D / H), as isotope delta δD value, and reported in per mill (‰):

$$\delta D = \frac{R_{\text{sample}}\,(\text{D/H})}{R_{\text{standard}}\,(\text{D/H})} - 1. \tag{1}$$

The isotopic standard is Vienna Standard Mean Ocean Water (VSMOW). H_2 mole fractions are reported as mole fractions in nmol mol^{-1}, abbreviated ppb (10^{-9}, parts per billion) and linked to the MPI2009 calibration scale for atmospheric hydrogen (Jordan and Steinberg, 2011). As working standards, atmospheric air from laboratory reference air cylinders and synthetic air mixtures were used (Walter et al., 2012, 2013; Batenburg et al., 2011); the H_2 mole fractions of the air in these cylinders were determined by the

Max Planck Institute for Biogeochemistry, Jena, Germany. The atmospheric reference air and the synthetic isotope reference air were measured daily (atmospheric reference air at least twice) and results were used for correction of the sample measurements. The uncertainties reported here reflect random (i.e., repeatability) errors only and do not include possible systematic errors (Batenburg et al., 2011; Walter et al., 2012, 2013). Samples were measured in random order and analyzed within 3 months (ANT-XXIV/4, ANT-XXV/5, ANT-XXVI/1) up to 2 years (ANT-XXVI/4) after sampling. Storage tests indicate that glass flasks equipped with Kel-F valves are stable for H_2 (Jordan and Steinberg, 2011). The mean measurement repeatability between the two measurements on the same flask was between ±3.2 (ANT-XXV/5, $n = 14$) and ±6.4 ppb (ANT-XXVI/4, $n = 108$) for the mole fraction and ±3.4 ‰ (ANT-XXVI/4, $n = 108$) and ±5.0 ‰ (ANT-XXV/5, $n = 14$) for the isotopic composition.

H_2 and CO mole fractions were also measured by using a Peak Performer 1 RGA (Reduced Gas Analyzer) with synthetic air as a carrier gas, either continuously on-board (ANT-XXVI/4, see Sect. 2.4.2) or from discrete flasks in the laboratory (ANT-XXV/5 and ANT-XXVI/1). The discrete RGA measurements were performed from the same glass flasks after measurement of the isotope system (see above). Due to a remaining slight overpressure in the flasks, an active pumping of the air into the RGA was not necessary and the flasks were simply connected to the RGA inlet by Teflon tubing. The remaining pressure was mostly sufficient to perform 8 to 10 measurements. A slight memory effect was observed and thus only the last 5 measurements were taken into account when stable. Samples with only three or less valid measurements were not used for evaluation. The standards were the same as those used for the isotope system. For both cruises (ANT-XXV/5 and ANT-XXVI/1), the mean measurement repeatability was better than ±0.8 (H_2) and ±2 % (CO). A comparison between the H_2 mole fractions measured with the Peak Performer 1 RGA and the isotopic experimental setup reveals on average slightly lower RGA values of (7.5 ± 23.8) ppb (see Fig. 3).

2.4.2 Atmospheric H_2 measured continuously

For the on-board continuous measurements of H_2 mole fractions a Peak Performer 1 RGA was used. The atmospheric air was drawn from the bridge deck to the laboratory in 1/4 inch Decabon tubing. The CO mole fraction was also measured in the same measurement and will be reported here for information, but without further discussion.

In alternating order, 10 air samples and 10 aliquots of reference air were measured, using synthetic air as carrier gas. Due to small memory effects, only the last 5 measurements of each were taken into account when the values were stable. The mole fractions of H_2 and CO were calculated by using the mean of the enclosing standard measurements, with an estimated maximal error of ±5 %. For more details see Popa et al. (2014). The mean measurement repeatability for the air samples was ±1.7 % for H_2 and ±3.6 % for CO in ambient air, respectively ±0.8 (H_2) and ±0.9 % (CO) for the reference air. Comparing the H_2 mole fractions measured continuously on the RGA with discrete samples measured on the isotope system and collected close in time, we found a mean offset of (−18.8 ± 16.4) ppb for the RGA results.

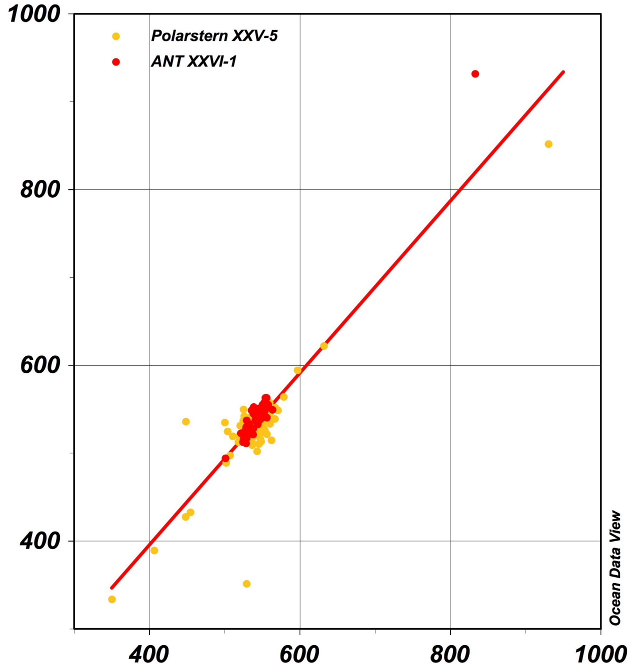

Figure 3. Comparing the H_2 mole fractions (ppb) measured with the isotopic experimental setup (x axis) and the Peak Performer 1 RGA (y axis) during ANT-XXVI/1 (red labeled) and ANT-XXV/5 (yellow labeled), $y = 0.979x + 3.96$, $R^2 = 0.81$, $n = 147$.

2.4.3 Dissolved H_2 extracted from surface water

The discrete samples of extracted dissolved H_2 were measured as described for the discrete atmospheric samples in Sect. 2.4.1. Details about assumptions and calculations to determine dissolved H_2 concentrations and isotope delta values and quantity symbols are given in detail in the Supplement.

We define the extraction efficiency η as

$$\eta = \frac{c_\mathrm{h} V_\mathrm{h}}{c_\mathrm{w0} V_\mathrm{w}}, \tag{2}$$

where V_h and V_w are the volume of the headspace and the water fraction, and c_h the concentration of H_2 in the headspace. The initial concentration of H_2 in seawater, c_w0, can be calculated from

$$c_\mathrm{w0} = \frac{c_\mathrm{h} V_\mathrm{h}}{\eta V_\mathrm{w}}. \tag{3}$$

The concentration in the headspace, c_h, was not measured directly, but can be derived from the measured H_2 mole fraction in the sampling flask. The sampling procedure following gas extraction under vacuum can be broken into three steps (see Methods section):

1. expansion of the headspace into the gas transfer system
2. addition of makeup gas
3. expansion of the headspace / makeup gas mixture into a sample flask.

As shown in the Appendix, the original concentration of H_2 in seawater (in $\mathrm{nmol\,L^{-1}}$) can be calculated using the following equation

$$\eta c_{\mathrm{w0}} = \frac{y_{\mathrm{f}}\left[\left(1+\frac{V_{\mathrm{t}}}{V_{\mathrm{h}}}\right)p_{\mathrm{htm}} - p_{\mathrm{h}}(\mathrm{H_2O})\right] - y_{\mathrm{m}}\left[\left(1+\frac{V_{\mathrm{t}}}{V_{\mathrm{h}}}\right)p_{\mathrm{htm}} - p_{\mathrm{h}}\right]}{V_{\mathrm{w}}\mathrm{RT}}, \tag{4}$$

where y_{f} is the dry mole fraction of the air in the flask and y_{m} the mole fraction of the makeup gas $= (543.9 \pm 0.3)$ ppb.

The extraction efficiency, η can be calculated from the following mass balance

$$V_{\mathrm{w}}c_{\mathrm{w0}} = V_{\mathrm{h}}c_{\mathrm{h}} + \alpha V_{\mathrm{w}}c_{\mathrm{h}}. \tag{5}$$

Assuming that headspace gas phase and water phase are in equilibrium, the ratio of the H_2 concentration in water and in the headspace is given by the Ostwald coefficient (Battino, 1984) (where the concentrations refer to in situ temperature):

$$\alpha = \frac{c_{\mathrm{w}}}{c_{\mathrm{h}}}. \tag{6}$$

This gives for the extraction efficiency as defined in Eq. (2)

$$\eta = \left(1 + \alpha\frac{V_{\mathrm{w}}}{V_{\mathrm{h}}}\right)^{-1}. \tag{7}$$

In the present case, $\alpha = \alpha(\mathrm{H_2})$ was equal to 0.0163 ± 0.0001, which gives $\eta = 92.12$ $(\pm 0.013)\,\%$ for $V_{\mathrm{w}}/V_{\mathrm{h}} = 8.4/1.6 = 5.25$.

Two alternative scenarios were considered to derive the δD of the dissolved H_2, with scenario 1 assuming equilibrium isotopic fractionation between headspace and water, and scenario 2 assuming kinetic isotopic fractionation during extraction from Niskin bottle to glass vessel.

$$\text{Scenario 1}: \delta_{\mathrm{w0}} = \delta_{\mathrm{h}} + \varepsilon\,(1-\eta)\,(1+\delta_{\mathrm{h}}) \tag{8}$$

The equilibrium isotope fractionation between dissolved phase and gas phase is $\varepsilon = (37 \pm 1)$ ‰ at 20 °C (Knox et al., 1992).

$$\begin{aligned}\text{Scenario 2}: \delta_{\mathrm{w0}} &= \frac{(1+\delta_{\mathrm{h}})\,\eta}{1-(1-\eta)^{1+\varepsilon_{\mathrm{k}}}} - 1 \\ &\approx \delta_{\mathrm{h}} + \varepsilon_{\mathrm{k}}\,(1-\eta)\,(1+\delta_{\mathrm{h}})\,\frac{\ln(1-\eta)}{\eta}\end{aligned} \tag{9}$$

The kinetic isotope fractionation during gas evasion is $\varepsilon_k = (-18 \pm 2)$ ‰ at 20 °C (Knox et al., 1992). The approximation is not used and only shown to illustrate the small difference between δ_{w0} and δ_{h} when $\eta \approx 1$.

The temperature dependences of ε and ε_k are unknown and were neglected here.

The air saturation equilibrium concentration, $c_{\mathrm{sat}}(\mathrm{H_2})$, was determined using the parameterization of Wiesenburg and Guinasso (1979). The H_2 saturation anomaly, $\Delta(\mathrm{H_2})$, was calculated as the difference between the measured H_2 concentration, $c(\mathrm{H_2})$, and $c_{\mathrm{sat}}(\mathrm{H_2})$:

$$\Delta(\mathrm{H_2}) = c(\mathrm{H_2}) - c_{\mathrm{sat}}(\mathrm{H_2}). \tag{10}$$

Meteorological and oceanographic parameters (radiation, air and water temperatures, salinity, relative humidity) were measured using standard instrumentation and recorded and provided by the data system of the ships. More information about devices and sensor documentation can be found on the website of the Alfred Wegener Institute http://dship.awi.de/. Backward trajectories were calculated using the backward "Hybrid Single Particle Lagrangian Integrated Trajectory" (HYSPLIT, Schlitzer, 2012) model of the National Oceanic and Atmospheric Administration (NOAA, http://ready.arl.noaa.gov/HYSPLIT.php).

2.5 Modeling

2.5.1 TM5 model

We performed simulations of H_2 mole fractions and isotopic composition with the global chemistry transport model TM5 (Krol et al., 2005), and compared them with our measurement data (Fig. 5). The simulation setup was similar to the one of Pieterse et al. (2013) and only a short description is given here. The model version used employs the full hydrogen isotopic scheme from Pieterse et al. (2009) and uses ERA-Interim meteorological data. The chemistry scheme is based on CBM-4 (Houweling et al., 1998), which has been extended to include the hydrogen isotopic scheme (that is, for all chemical species that include hydrogen atoms, HH and HD are treated separately and have different reaction rates). The H_2 sources and isotopic signatures are given as input; these and also the H_2 soil deposition velocities are identical to Pieterse et al. (2013).

The model has a relatively coarse spatial resolution of 6° longitude by 4° latitude, and a time step of 45 min. Daily average mole fraction fields are used for comparison to observations. The model results were interpolated to the time and location of the observations.

2.5.2 Global oceanic emissions

The climatological global oceanic emissions were calculated using the protocol of Pieterse et al. (2013), based on the GEMS database and an assumed mean oceanic H_2 source of $5\,\mathrm{Tg\,a^{-1}}$ as given from global budget calculations (see Ehhalt and Rohrer, 2009, and references therein, Pieterse et al., 2013). The spatial and temporal variability of oceanic H_2 emissions caused by N_2 fixation are adopted from the spa-

Table 2. Hemispheric means of atmospheric H_2 and its isotopic composition along the four meridional Atlantic transects.

		Southern Hemisphere				Northern Hemisphere			
Cruise		IRMS – H_2 mole fraction (ppb)	δD (‰)	RGA – H_2 mole fraction (ppb)	RGA – CO mole fraction (ppb)	IRMS – H_2 mole fraction (ppb)	δD (‰)	RGA – H_2 mole fraction (ppb)	RGA – CO mole fraction (ppb)
ANT-XXI/4	mean	543.4 ± 7,3	145.4 ± 5,3	No data	No data	544.1 ± 9.8	118.6 ± 3.9	No data	No data
April 2008	range	528.8–568.5	135.4–155.7			522.0–567.8	110.4–130.9		
	n	49 (2 values excluded)	49 (2 values excluded)			44	44		
ANT-XXV/5	mean	533.9 ± 38.7	140.5 ± 21.1	520.4 ± 24.0	59.9 ± 17.7	532,94 ± 19,73	121,28 ± 7,09	526.18 ± 12.6	112.67 ± 21.3
April 2009	range	350.2–631.9	20.9–166.1	432.5–545.1	43.6–119.6	466.9–560.3	89.1–130.9	508.9–564.1	76.9–190.5
	n	60	60	21	21	28 (2 values excluded)	28 (2 values excluded)	29	29
ANT XXVI/1	mean	548.5 ± 6.8	143.2 ± 4.2	546.4 ± 7.4	59.9 ± 10.5	532,04 ± 10,65	133,94 ± 4,43	526.02 ± 10.53	76.73 ± 7.43
October 2009	range	535.9–563.4	135.5–149.3	531.4–563.0	47.7–85.8	501.1–551.7	123.5–141.7	494.2–548.8	65.4–96.1
	n	30 (1 value excluded)	30 (1 value excluded)	49	49	29	29	46	46
ANT XXVI/4	mean	541.6 ± 16.3	143.7 ± 11.5	525.1 ± 29.1	47.2 ± 8.8	539.4 ± 14.8	116.2 ± 11.5	507.8 ± 15.7	120.8 ± 11.2
April 2010	range	496.0–579.6	89.3–161.8	481.5–696.8	36.2–121.8	505.5–564.6	93.8–146.6	481.3–603.8	72.7–146.1
	n	58	58	617	617	56	56	1339	1339

tial and temporal distribution of oceanic CO (Erickson and Taylor, 1992).

3 Results and discussion

3.1 Atmospheric H_2 transects

Our data set includes data of two hemispheres and two seasons between 2008 and 2010 (see Table 2, Fig. 4). The mean mole fraction of H_2 ranged between (532.0 ± 10.7) and (548.5 ± 6.8) ppb. In spring, the mean values were almost equal between the hemispheres with approximately 1 to 2 ppb difference, but they differed significantly in autumn. In this season, the mean values in the Northern Hemisphere (NH) were approximately 16 ppb or 3 % lower compared to the Southern Hemisphere (SH), with a distinct transition between the hemispheres at around 8° N. In contrast, δD differed significantly between the hemispheres in both seasons. In the Southern Hemisphere, absolute δD values were always between 9 and 27 ‰ higher than in the Northern Hemisphere, and generally remained within a narrow range between (140.5 ± 21.1) and (145.4 ± 5.3) ‰. In contrast to the mole fraction, isotope delta differences between the hemispheres were less pronounced in autumn than in spring. These two seasonal patterns, in the following defined as "summer signal" and "winter signal", are mainly caused by biological processes and tropospheric photochemistry and driven by variations in the NH. They are in line with previously published data and model results (Rhee et al., 2006; Price et al., 2007; Rice et al., 2010; Pieterse et al., 2011, 2013; Batenburg et al., 2011; Yver et al., 2011; Yashiro et al., 2011).

The "summer signal", observed in October, is characterized by lower H_2 mole fractions in the Northern Hemisphere and a less pronounced difference in δD between the hemispheres. Deposition by biological activity of microorganisms in the soils is the main sink of H_2 (Yonemura et al., 2000; Pieterse et al., 2013) and the sink strength in the Northern Hemisphere and the Southern Hemisphere depends on the distribution of landmasses and on season. With approximately 70 % of landmasses in the NH and higher microbial activity in the summer, the mole fraction during this season is lower in the NH than in the SH. Due to the general preference of organisms for molecules with lighter isotopic composition, the δD values increase during summer in the NH and the interhemispheric gradient becomes less pronounced.

The "winter signal" observed in April is defined by almost equal mole fractions and more pronounced differences in δD values between the hemispheres. In winter, molecular hydrogen is accumulating in the NH hemisphere, and the main source is fossil fuel combustion with a depleted isotopic composition of −170 to −270 ‰ (Gerst and Quay, 2001; Rahn et al., 2002). This leads to nearly equal mole fractions in both hemispheres and a more pronounced δD gradient, with isotopically lighter H_2 in the NH. The contribution of source and sink processes in the SH to the seasonal patterns is less pronounced than for the NH (Pieterse et al., 2011, 2013). As a result, the H_2 seasonal cycle in the SH is much weaker compared to the NH. The SH isotopic H_2 signature is caused by mainly emissions and chemical loss with an isotope delta of approximately +190 ‰, which explains the generally higher δD values. The Intertropical Convergence Zone (ITCZ) separates the two hemispheres and is clearly visible, not only in the H_2 distribution, but also in the CO distribution.

Simulations of H_2 mole fractions and isotopic composition using the global chemistry transport model TM5 (Krol et al., 2005) compared with our atmospheric data reveal that the model simulates the H_2 mole fractions quite well (Fig. 5), with a slight overestimate of up to 20 ppb (which means up to 4 %).

The model results are less variable on small spatial scales, due to the low spatial resolution, and possibly to local influences that are not included in the model (e.g., ocean emis-

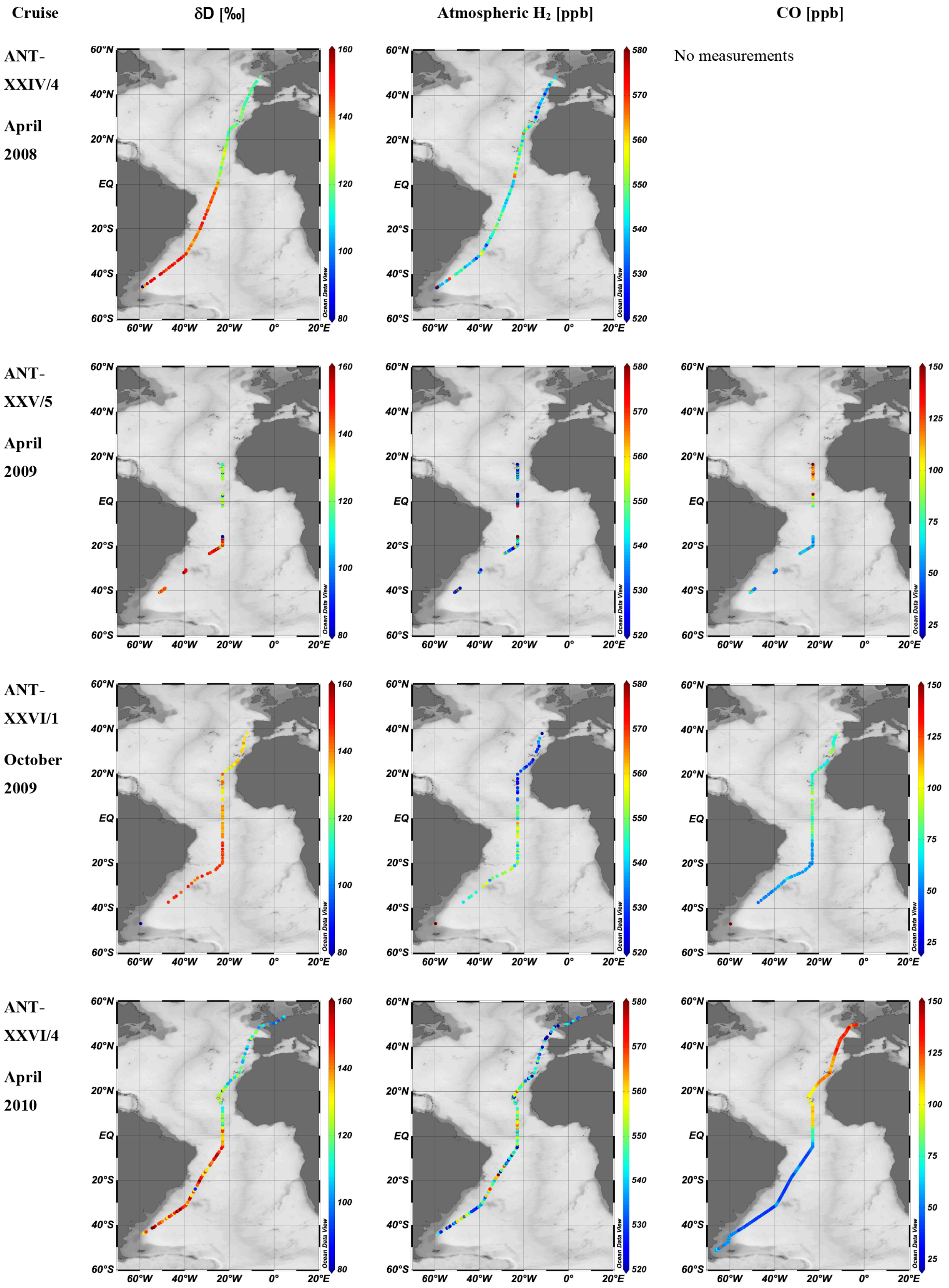

Figure 4. δD (H_2) (‰) (first column), H_2 mole fraction (ppb) (second column), and CO mole fraction (ppb) (third column), along the meridional cruise tracks of RV *Polarstern*, the mole fraction and δD of H_2 are measured by IRMS, the CO mole fraction by RGA.

Table 3. Overview of means of atmospheric H_2 and its isotopic composition along the five high–resolution transects of ANT-XXV/5, including the standard deviation and the range.

Transect (latitude)		Mole fraction (ppb)	δD (‰)
40.8° S/38.9° S	mean	515.5 ± 37.7	141.4 ± 6.2
$n = 12$	range	448.4–566.9	129.3–151.0
33.0° S/30.8° S	mean	521.4 ± 53.3	152.9 ± 5.9
$n = 12$	range	350.2–551.9	142.8–166.1
23.5° S/15.7° S	mean	536.9 ± 38.4	144.1 ± 41.4
$n = 32$	range	392.9–631.9	20.91–322.45
2.0° S/3.2° N	mean	537.5 ± 36.2	119.5 ± 12.6
$n = 11$	range	466.9–592.2	89.1–135.5
9.9° N/16.2° N	mean	537.0 ± 12.2	122.5 ± 3.0
$n = 21$	range	511.0–560.3	118.4–131.0

sions in the model are less variable in time and space than they could be in reality). The largest differences between the modeled and measured H_2 occur between 30° S and the equator. This seems a systematic feature and could be due to a slight overestimation of sources or underestimation of sinks by the model. Despite these small differences, the model is consistent with measured H_2 mole fractions and simulates them well. Large-scale features are clearly visible, like the sharp gradient around 10° N during cruise ANT-XXVI/1 (Fig. 5, top, third plot), or the decrease in δD towards northern mid-latitudes (most evident for the cruises ANT-XXIV/4 and ANT-XXVI/4, first and last plots in Fig. 5, top). A slight overestimate of the H_2 mole fractions was also noted by Pieterse et al. (2013). This might be explained by an overestimate of photochemical sources in the model, which would influence only the mole fractions but not the δD values.

The model simulates the isotopic composition of H_2 even better than the mole fractions. The most important features are the general decrease from south to north, and the sharp gradient around the equator. As most sources and sinks of H_2 have very different isotopic signatures, this good comparison indicates that the model adequately represents both the magnitude and the isotopic signature of the main components of the H_2 cycle. Similar to Pieterse et al. (2013) we also observe a slight underestimate of the δD at high southern latitudes, which is possibly due to underestimating the isotopic composition assumed for H_2 returning from the stratosphere in the latitude band 60 to 90 °S.

3.2 Spatial and temporal high–resolution transects during ANT-XXV/5

In April 2009 the sampling resolution was increased to approximately one sample per 2 h for five selected sections of the transect during ANT-XXV/5 (Fig. 4, Table 3): three in the Southern Hemisphere, one crossing the equator and one in the Northern Hemisphere. These transects were chosen based on previously published data (Herr et al., 1984; Conrad and Seiler, 1988) and with the aim to get an indication of small-scale sources or diurnal cycles of atmospheric H_2 for further investigations.

All transects showed neither a diurnal cycle nor a correlation with radiation and a range of δD values within or only slightly outside a 2σ range around the mean, except for the one between 23.5 to 15.7° S (Fig. 6a). Here the highest H_2 mole fractions of (631.9 ± 3.2) ppb, combined with the lowest δD values of (20.9 ± 5.0) ‰, were found around 16° S. Due to the limited spatial resolution and therefore low number of data points, a Keeling plot analysis (Fig. 6b) of the data between 15 and 18° S was made with either 5, 7, or 9 data points to get a reasonable range for the source signature. It reveals a mean source signature of −561.5 in a range of −530 to −683 ‰ ($n = 7 \pm 2$, $R^2 = 0.85 \pm 0.01$). The correlation coefficient is a mean of the three analyses.

HYSPLIT trajectories for the samples collected on this transect during the 28 April 2010 and 1 May 2010 (21.8 to 15.7° S) reveal the same origin of air masses coming from the direction of Antarctica. Oceanographic parameters such as water temperature and salinity are similar and do not correlate with H_2 mole fractions and δD values. These findings indicate a strong but local source, and the low δD value for the source obtained by the Keeling plot analysis points to biological production (Walter et al., 2012). Such local and temporal patchiness of high H_2 mole fractions in surface waters was reported previously in correlation to high N_2 fixation rates (Moore et al., 2009, 2014). Although reported for other oceanic regions, the H_2 mole fractions and δD values here neither show a diurnal cycle (Herr et al., 1984), nor are they correlated with radiation indicating photochemical production (Walter et al., 2013), and most of the values were observed during night. Wilson et al. (2013) recently showed that H_2 production and uptake rates clearly depends on microbial species, and also on their individual day-night rhythm, but the contribution of different diazotrophs to the marine H_2 cy-

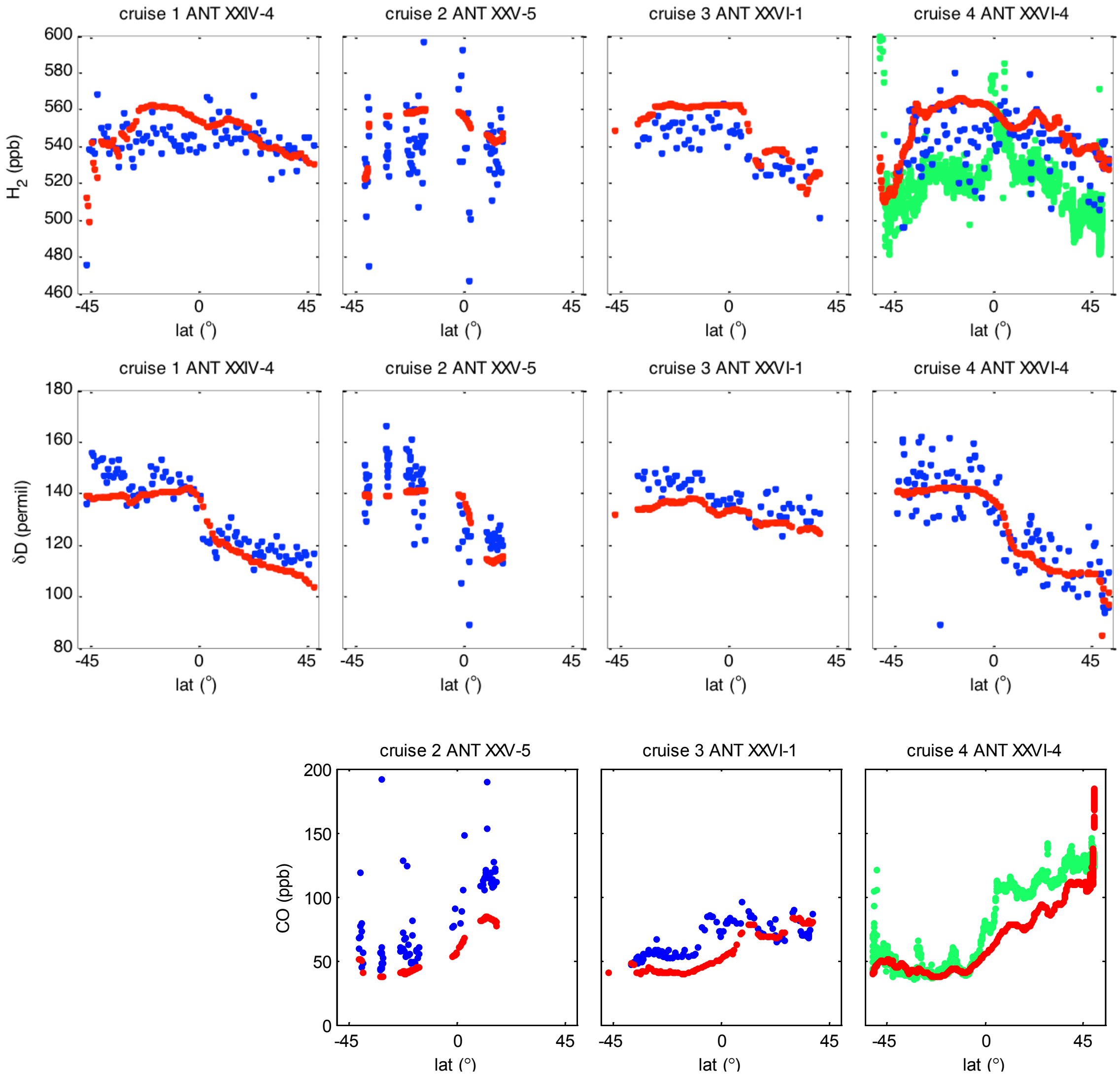

Figure 5. Comparison of measurement results of H_2 and CO mole fractions and δD with TM5 model results (given in red). Data are shown against latitude. The blue markers show results of flask samples, and the green markers represent the continuous in situ measurements (performed with the peak performer instrument on–board). CO has not been analysed in the flasks sampled during the last cruise. The model data were interpolated at the place and time of sampling or measurements.

cle is unknown (e.g., Bothe et al., 2010; Schütz et al., 2004; Wilson et al., 2010a, b; Punshon and Moore, 2008b; Scranton 1983, Moore et al., 2009).

Around 21.2° S one single sample with a low mole fraction of (393.9 ± 3.2) ppb in combination with a high δD of (322.45 ± 5) ‰ value was observed. As mentioned before HYSPLIT models reveal the same origin of air masses on this transect, thus this sample indicates probably a local sink. However, this interpretation depends on only one single measurement point and although neither instrumental parameters indicated an outlier nor meteorological or oceanographical parameters differed from other samples, we cannot exclude an artefact due to sampling, storage, or analyses. A simple Rayleigh fractionation model reveals a fractionation factor of $\alpha = 0.646 \pm 0.002$, which is close to the value of oxidation by HO$^\bullet$ ($\alpha = 0.58 \pm 0.07$, Batenburg et al., 2011). An estimate of the δD value by using an HO$^\bullet$ oxidation fractionation factor would lead to an increase by 125 or 149 ‰, respectively. The observed increase of δD seems reasonable when assuming oxidation by HO$^\bullet$, but with respect to the HO$^\bullet$ mole fraction and the slow reaction rate of H_2 + HO$^\bullet$, it is questionable whether the H_2 decrease here can be explained by this.

3.3 Dissolved H_2

A new method has been presented to extract H_2 from surface waters for isotopic determination. Before discussing the

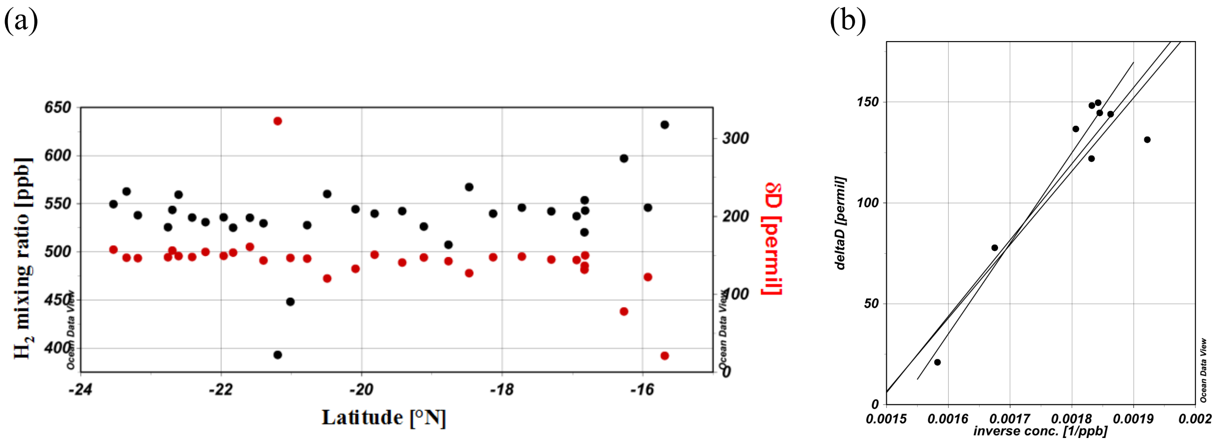

Figure 6. (a) H_2 mole fraction (ppb) (black) and δD [‰] (red) along the ANT-XXV/5 high–resolution transect 24–15° S; **(b)** Keeling plot of the samples along the high–resolution transect north of 18° S. The three trend lines indicate the range of the Keeling plot analysis that was applied to determine the source signature.

measurement results, we will give an overview of the possible main errors and their effects. To show the effect of the errors on the measurements, we will present error factors, thus how much the final data differ by shifting the respective parameter by 1 % and also the absolute assumed error.

For the extraction method several error sources could be identified: the determination of pressure, especially in the sampling vessel before adding the make-up gas and during extraction, the temperature of air and water, respectively the difference between them when the sample is extracted from the headspace, and the volume of the set-up and the sample. The determination of pressure in the sampling vessel would be one issue of further improvement, because the error caused by pressure deviations for the total pressure after adding the make-up gas is about a factor of 0.7 for concentrations and 0.2 for the isotopic values. The error based on temperature of air, water and sample is negligible due to high-precision measurements and the short handling time between water sampling and headspace extraction. The error for the volume parameter for the set-up is negligible due to the high volume, the precise determination of the glass vessel volume by weighing, and the calculation of the tubing volume. The main error source is the water volume of the sample, which counts by a factor of 5.9 for the concentration, but with negligible effect on the isotopic values. Although the relative error factor is quite high, the absolute value is assumed to be around 0.5 % due to the sample size, which has also been weighed at the home lab. The H_2 measurement procedure is the same as for atmospheric samples and possible errors are described in the respective sessions or related literature. However, the error caused by the determination of the dry mole fraction itself seems to have the main input by a factor of 5.3 for concentration and 4.6 for the isotopic values of dissolved H_2. Errors of the determination of the isotopic value are much less significant and count by a factor of 0.2.

Taking measurement and handling errors during the extraction as well as errors in the determination of the dry mole fraction into account, we assume a robust overall uncertainty of ±6.9 % for the dissolved H_2 mole fractions and ±4.7 % for the isotopic values by calculating the root of the sum of the squared uncertainties.

As shown in Table 4 we also tested the effect of equilibrium isotopic fractionation and kinetic isotopic fractionation. The effect is less than 0.2 %.

Therefore, recommendations for the extraction method are to additionally measure parameters such as the initial pressure in the glass vessel and to ensure a precise determination of the sample volume. Besides this we recommend high–precision IRMS measurements and to consider multiple sampling for better statistics on the data.

3.3.1 H_2 concentration

In total, 16 headspace samples were taken during the RV *Polarstern* cruise in April/May 2010 along the transect 32.53° W/18.79° S to 13.00° W/36.54° N and 6 samples during the RV *L'Atalante* cruise in February 2008 between 23.00–17.93° W to 16.9–19.2° N to analyze the H_2 mole fraction and the isotopic composition (see Table 4).

Although our setup was a prototype with possibilities for improvement, the mole fractions are in line with previously published data. The H_2 excess, $\Delta(H_2)$, exceeds 5 nmol L^{-1}, the saturation differ from close to equilibrium to 15-fold supersaturation. Highest supersaturation was found in the Southern Hemisphere between 16 and 11° S and in the Northern Hemisphere around the Cape Verde islands and the coast of Mauritania (Fig. 7a, Table 4).

Herr et al. (1984) reported patchy enhanced H_2 concentrations in the surface water with up to 5-fold supersaturation in the subtropical south Atlantic (18–31 and 29–42° W). This is comparable to what Conrad and Seiler (1988) found in the

Table 4. Overview of headspace sample results from the ANT-XXVI/4 cruise (2010) and the *L'Atalante* ATA-3 (2008),: χ_h is the measured mole fraction of the headspace in parts per billion (ppb = nmole mole^{-1}), χ_a is the corresponding atmospheric mole fraction in ppb, δD_h and δD_a is the measured isotopic composition in permil (‰). The H_2 equilibrium concentration $c_{sat}(H_2)$ was determined by using the equations from Wiesenburg and Guinasso (1979), the initial dissolved H_2 concentration c_{w0} is calculated as given in Supplement 1, and the excess ΔH_2 is the difference between them. $\delta_{w0\ SC1}$ and $\delta_{w0\ SC2}$ show the two scenarios to derive the initial isotope delta of dissolved H_2. $S_{(H_2)}$ is the saturation of H_2 in the surface water. The calculated extraction efficiency was 92.12 (±0.013)%. The calculations are given in the Supplement in more detail.

Date/Time (UTC)	Sampling position	χ_a (ppb)	δD_a (‰)	χ_h (ppb)	δD_h (‰)	$c_{sat}(H_2)$ (nmol L^{-1})	c_{w0} (nmol L^{-1})	$\Delta(H_2)$ (nmol L^{-1})	$\delta_{w0\ SC1}$ (‰)	$\delta_{w0\ SC2}$ (‰)	$S_{(H_2)}$ (%)
21.04.2010 15:15	−18.79° N −32.53° E	562.0	148.5	653.3	−37.3	0.35	1.68	1.32	−536.2	−535.6	475
22.04.2010 15:24	−15.91° N −30.49° E	524.2	134.5	750.6	−138.6	0.33	2.89	2.57	−654.8	−654.4	880
23.04.2010 15:21	−13.06° N −28.51° E	551.6	144.3	754.4	−125.1	0.35	2.91	3.57	−602.9	−602.5	841
24.04.2010 15:36	−10.71° N −26.92° E	522.0	153.2	797.0	−151.2	0.33	3.52	3.19	−605.6	−605.2	1074
25.04.2010 15:24	−7.97° N −25.02° E	542.9	154.7	674.8	−59.4	0.34	1.97	1.63	−566.1	−565.6	581
26.04.2010 15:12	−5.16° N −23.11° E	517.8	149.7	584.5	9.2	0.32	0.83	0.51	−654.0	−653.6	256
28.04.2010 13:54	1.78° N −23.00° E	540.9	144.4	619.8	−33.1	0.34	1.27	0.93	−682.1	−681.8	376
29.04.2010 14:21	4.99° N −23.00° E	562.8	114.2	615.9	−11.7	0.35	1.25	0.89	−575.4	−574.9	353
30.04.2010 14:15	8.07° N −23.00° E	550.6	118.6	591.1	−0.6	0.35	0.94	0.60	−680.8	−680.5	271
02.05.2010 14:39	14.55° N −23.68° E	541.3	110.5	603.3	−15.0	0.35	1.13	0.78	−680.7	−680.4	324
04.05.2010 13:39	17.61° N −24.75° E	523.2	121.5	686.5	−83.6	0.34	2.27	1.93	−630.8	−630.3	674
05.05.2010 13:21	20.26° N −22.86° E	559.0	125.7	667.9	−55.3	0.36	2.05	1.69	−572.6	−572.2	566
06.05.2010 12:30	23.12° N −20.66° E	550.7	104.3	586.6	−1.1	0.36	0.93	0.57	−719.3	−719.0	258
07.05.2010 12:18	26.07° N −17.50° E	539.8	108.9	575.3	20.3	0.35	0.79	0.43	−645.2	−644.8	221
09.05.2010 12:51	33.60° N −13.86° E	546.8	104.6	624.2	21.0	0.37	1.51	1.14	−327.2	−326.4	410
10.05.2010 12:55	36.53° N −13.01° E	531.8	107.8	571.6	62.0	0.36	0.77	0.41	−230.2	−229.3	213
09.02.2008 16:05	16.91° N −16.82° E	527.2	118.4	141.7	−224.09	0.35	1.57	1.22	−221.8	−221.0	446
11.02.2008 17:58	18.77° N −16.81° E	538.5	115.3	550.4	−383.39	0.36	5.91	5.54	−381.6	−380.9	1628
15.02.2008 10:27	17.93° N −16.38° E	536.8	112.2	138.8	−114.85	0.36	1.79	1.42	−112.2	−111.3	492
16.02.2008 6:05	17.72° N −16.69° E	548.4	120.0	20.3	−180.51	0.37	0.50	0.13	−179.0	−178.2	135
16.02.2008 17:41	18.01° N −17.01° E	548.4	120.0	31.0	−218.73	0.37	0.72	0.35	−217.3	−216.5	194
18.02.2008 18:22	18.00° N −23.00° E	541.8	126.5	48.9	−321.61	0.36	1.16	0.80	−320.4	−319.7	322

southern Atlantic, on a similar cruise track as the RV *Polarstern*. Around the equator they measured H_2 surface water concentrations up to 12-fold supersaturation. In the southern Pacific, Moore et al. (2009) combined H_2 surface water measurements with N_2 fixation measurements. They reported a strong correlation between these parameters, a patchy distribution and a steep maximum of H_2 concentrations up to 12.6 nmol L^{-1} around 14° S.

The recently published data by Moore et al. (2014) show similar patterns across the Atlantic as we found, with highest values around the southern and northern subtropics. However, our saturations are lower than the ones given by them, especially in the Northern Hemisphere. Such differences

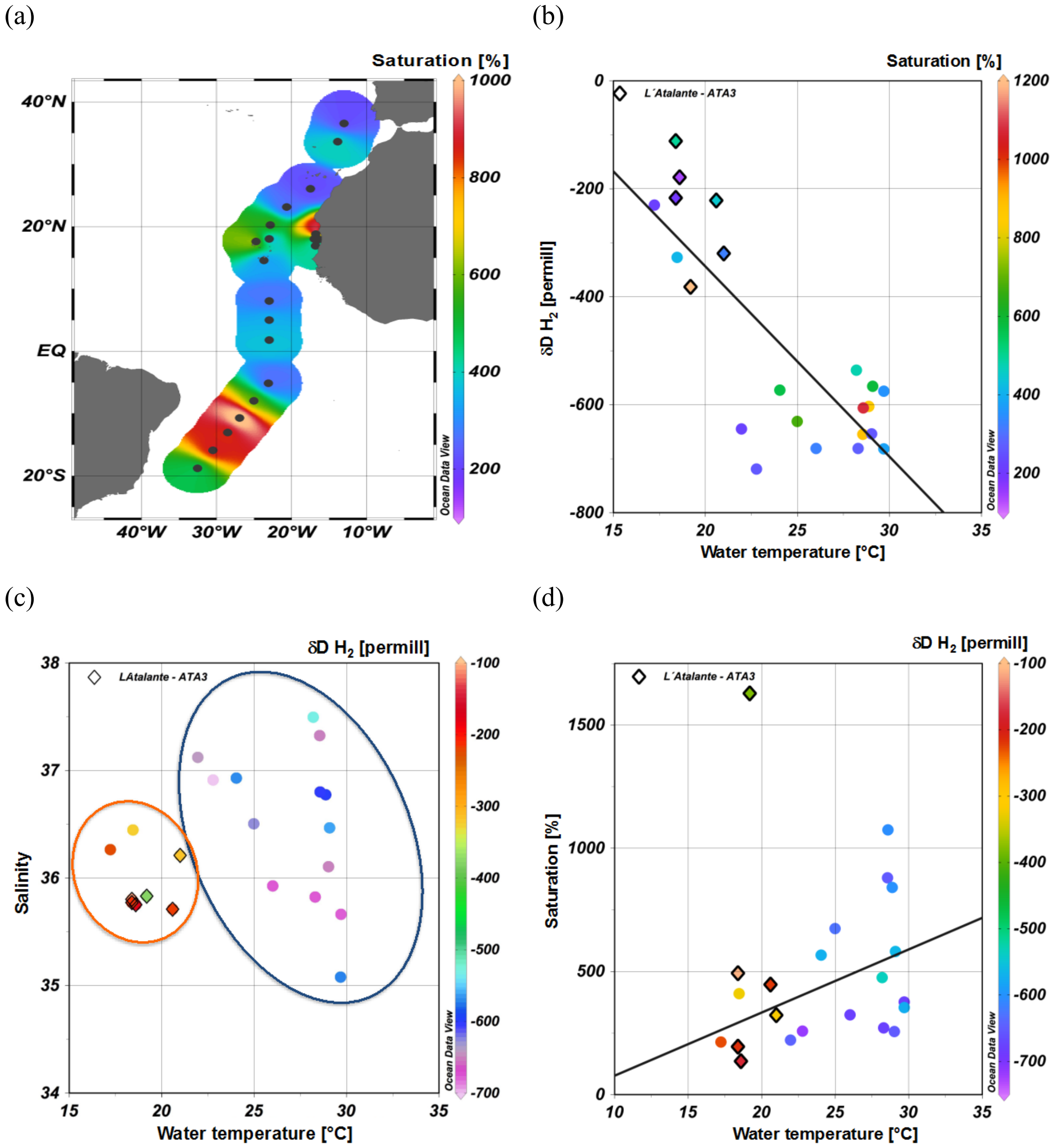

Figure 7. (a) H_2 saturation in the surface water (color coded) along the RV *Polarstern* cruise track of ANT-XXVI/4 and the RV *L'Atalante* cruise ATA-3, with maxima around the Cape Verde islands and 10–15° S, Note: each sample is represented by a single dot. **(b)** Comparing the δD (H_2) at different water temperatures, the respective H_2 saturation are color coded, sample dots marked with a diamond belong to the RV *L'Atalante* cruise, sample dots without to the ANT-XXVI/4 cruise; $y = -35.2x + 360.9$, $R^2 = 0.66$, $n = 22$. **(c)** Distribution of δD (H_2) (color coded) in correlation between water temperature and salinity. **(d)** Correlation between water temperature and H_2 saturation, the δD (H_2) is color-coded, the exceptional high saturation has been excluded from the correlation calculation, $y = 0.26x - 2.79$, $R^2 = 0.22$, $n = 21$.

might be caused by experimental issues such as overestimated extraction efficiency or can be due to real temporal variability as the sampling seasons differed. The extraction efficiency has been estimated as 92.12 (±0.013) % (see Supplement) and was incorporated into the calculation of the original seawater concentration. With respect to the assumption of biological production as main production pathway it is more likely that due to the different sampling seasons less H_2 was produced in April than in October/November because of less microbial activity especially on the Northern Hemisphere in boreal winter.

3.3.2 Isotopic composition of H_2

Additional information about H_2 sources comes from the analysis of the H_2 isotopic composition. In the literature, only one experimental value of dissolved marine δD exists, $\delta D = -628$ ‰ (Price et al., 2007; Rice et al., 2010), but the origin of this value is unclear and it is based on unpublished data. Nevertheless, this value has been used as representative for oceanic emission in several global budget calculations (e.g., Price et al., 2007; Pieterse et al., 2011). Other authors (e.g., Rahn et al., 2003; Rhee et al., 2006) used a theoretical value of -700 ‰, as expected for thermodynamic isotope equilibrium between H_2 and H_2O based on the calculations of Bottinga (1969). The results presented here are the first well-documented experimental results for isotope analysis of dissolved H_2 in seawater.

From the measurement of the isotopic composition of H_2 in the headspace we calculate the isotopic composition of H_2 that was originally dissolved in the sea water as described in Sect. 2.4.3 and in the Appendix, using two different assumptions for fractionation between dissolved H_2 and H_2 in the gas phase. The results shown in Table 4 reveal δD values for the dissolved H_2 that vary within a wide range of -112 to -719 ‰ for both fractionation scenarios. Interestingly, δD shows two distinct groups of samples that can be separated by the water temperature (Fig. 7b). In water masses with a temperature above 21 °C the δD values are (-629 ± 54) ‰ ($n = 14$), in water masses with a temperature of 20 °C or below δD values are (-249 ± 88) ‰ ($n = 8$). There is no correlation of δD with salinity (Fig. 7c), but the high temperature (and low δD) waters show also a generally higher saturation than the low temperature (high δD) waters (Fig. 7d).

The very depleted isotope signature of the H_2 in the warmer water masses is consistent with the values expected for biological production. The slight enrichment compared to the value of ≈ -700 ‰ that is expected for biologically produced H_2 in equilibrium with ocean water (Bottinga, 1969; Walter et al., 2012) may be caused by a partial consumption within the water, which would enrich the remaining fraction. The relatively smooth distribution of the isotopic composition of H_2 in the atmosphere strongly indicates that the contribution from atmospheric variability cannot be a main contributor of the isotope variations observed in dissolved H_2, even within the group of the depleted samples.

To our knowledge this is the first time that oceanic production of H_2 has been directly attributed to biological processes by using isotope techniques. For the samples collected from warm surface waters, our results verify the general assumption of a biological production process as a main source of oceanic H_2 to the atmosphere rather than photochemical or other sources (Herr et al., 1981; Conrad, 1988; Punshon and Moore, 2008; Moore et al., 2009). The dominance of biological formation at higher temperatures is qualitatively consistent with the general understanding of the temperature dependence of N_2 fixation rates for N_2 fixers such as e.g., *Trichodesmium* sp., which exhibit highest N_2 fixation rates within a temperature range between 24 to 30 °C (Breitbarth et al., 2007; Stal, 2009). In fact, the saturations also show a correlation with temperature, but less clear than for δD (Fig. 7d), presumably due to simultaneous uptake and consumption processes in a complex microbial community.

However, this clear attribution is only valid in water masses with higher temperatures and the unexpectedly high δD values in cooler waters indicate the influence of other processes. The isotopic enrichment that is expected for removal of H_2 (Chen et al., 2015; Rahn et al., 2003; Constant et al., 2016) is highly unlikely to cause a shift of almost 400 ‰ in δD from an assumed pure biological source, because in this case the removed fraction would have to be unrealistically large, as also recently argued for soil emitted H_2 (Chen et al., 2015). We suggest that a source of H_2 must exist in these surface waters, which produces H_2 that is out of isotope equilibrium with the water. This can be either one single source with an isotopic signature of approximately -250 ‰, or an even more isotopically enriched source that mixes with the depleted biological source.

Punshon and Moore (2008a, and references therein), reported abiotic photochemical H_2 production from CDOM and small organic compounds such as acetaldehyde or syringic acid. Walter et al. (2013) indicated, that biologically active regions such as the Banc d'Arguin at the coast of Mauritania could act as a pool of precursors such as VOCs for atmospheric H_2 with high δD values. It is thus possible that abiotic photochemical production in the surface water might be an alternative source of H_2 excess, which is not isotopically equilibrated with water, especially in regions with high radiation and biological activity, and less N_2 fixation. Given the fact that the two groups of warm and cold waters are relatively well separated and there is not a continuous mixing curve between two end members, the explanation of a single different source seems more straightforward. Isotope analyses are a powerful tool to distinguish this source from biological production. Additional measurements are needed to determine the isotopic signature of such a source and investigate to which extend photochemical production contributes to the oceanic H_2 budget in colder water masses, and also update the current models. However, with an isotopic signature of approximately -250 ‰, or an even more isotopically enriched, such a source would not significantly impact the current models.

Based on their H_2 measurements, Moore et al. (2014) suggested a substantial underestimation of oceanic N_2 fixation, especially due to high H_2 supersaturations measured in the Southern Hemisphere. By using direct measurements of N_2 fixation rates, a systematic underestimation by approximately 60 % was also proposed by Großkopf et al. (2012) who suggested a global marine N_2 fixation rate of (177 ± 8) Tg N a^{-1}. In order to identify a possible significant mismatch between N_2 fixation rates and total marine H_2 production, we calculated the climatological global

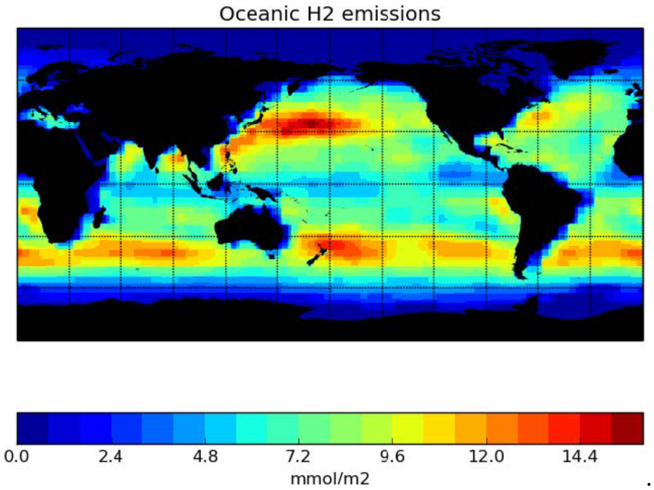

Figure 8. Oceanic H_2 emissions used in the TM5 model simulations (mmol m^{-2} a^{-1}, based on the distribution provided by the project GEMS (Global and regional Earth-system (atmosphere) Monitoring using Satellite and in-situ data) and scaled to a total oceanic source of 5 Tg a^{-1} (Pieterse et al., 2013)

oceanic emissions from the GEMS database using the protocol of Pieterse et al. (2013), and an assumed mean oceanic H_2 source of 5 Tg a^{-1} as given from global budget calculations. The estimated emission rates and distributions in the Atlantic Ocean (Fig. 8) are in line with the calculations of Moore et al. (2014), who reported H_2 sea-to-air fluxes mostly in the range of (10 ± 5) mmol, m^{-2} a^{-1} and an almost equal distribution between the hemispheres.

Westberry and Siegel (2006) estimated the global nitrogen fixation rate by *Trichodesmium* blooms by using satellite ocean color data at 42 Tg N a^{-1} and an additional 20 Tg N a^{-1} under non–bloom conditions, suggesting that *Trichodesmium* is likely the dominant organism in the global ocean new nitrogen budget. The good agreement between our measurements of H_2 concentrations and δD and the model results from the TM5 model indicate that the oceanic emissions of H_2 to the atmosphere are actually well represented in current atmospheric models (Pieterse et al., 2013 and references herein). The proposed underestimate of oceanic N_2 fixation and a possible additional H_2 release during this process seems already be incorporated in the current atmospheric budgets of H_2. Thus, supposing that both an assumed total oceanic H_2 source of 5 Tg a^{-1} to the atmosphere and a total global nitrogen fixation rate of approximately 177 Tg N a^{-1} are correct, our calculations clearly support the suggestion of Großkopf et al. (2012) that N_2 fixers other than *Trichodesmium* have been severely underestimated in the global picture and that the oceanic release ratio of H_2 to fixed N_2 clearly needs more attention. Besides *Trichodesmium*, several other N_2-fixing organisms are known for their potential to produce hydrogen (Wilson et al., 2010a; Falcón et al., 2002, 2004; Zehr et al., 2001; Kars et al., 2009; Barz et al., 2010), and even non-N_2-fixing organisms might play a role (Lilley et al., 1982).

4 Conclusions

Identifying sources is important to consider budgets and gain insight in production and consumption processes. Although H_2 has been assumed to be produced mainly biologically in the oceans, direct evidence was lacking. Our results verify a biological production as a main source of H_2 in oceanic surface water, especially in warmer water masses. As seen from the transects, local sources are difficult to spot due to their patchiness, this should be taken into account when planning the sampling strategy.

The unexpectedly high δD values in colder temperate water masses indicate the significant influence of processes other then biological production, and additional information, e.g., by isotopic composition is needed to distinguish and verify possible sources and supersaturations of dissolved oceanic H_2. Especially the investigation of the isotopic composition of possible production pathways such as abiotic photochemical H_2 production needs further attention and should be an upcoming issue.

The pattern of mole fractions and isotopic composition of H_2 along a north–south Atlantic transect clearly depends on season and hemisphere and is consistent with previous published data and models. A possible significant underestimation of N_2 fixation as assumed by several authors could – providing a net H_2 release rate – go along with higher H_2 emissions. However, a comparison with the TM5 model and the calculation of the climatological global oceanic emissions based on GEMS database reveal that the oceanic contribution to the global H_2 budget is reasonable and in general reproduced well; therefore, a proposed underestimation in the oceanic N_2 fixation seems already to be corrected (from atmospheric considerations) in the current atmospheric budgets of H_2. This also indicates, with respect to the proposed source different than biological production in colder temperate water masses, that such a source would probably not significantly impact the current models.

Besides the isotopic composition of photochemically produced H_2 the composition of N_2 fixer communities and the release ratio of H_2 to N_2 fixed needs more investigation to understand the general processes and distributions of oceanic H_2 in more detail.

The Supplement related to this article is available online at doi:10.5194/bg-13-323-2016-supplement.

Acknowledgements. We are very thankful to the crew of the RV *Polarstern* and RV *L'Atalante* for their friendly and professional help and support. This study was financed by the NWO (Netherlands Organization for Scientific Research), NWO project number 816.01.001, the EU FP7 project InGOS (GA number 284274), and the BMBF (Bundesministerium für Bildung und Forschung) project SOPRAN, grant FKZ 03F0462, grant 03F0611 and grant 03F0662.

Edited by: G. Hernd

References

Barz, M., Beimgraben, C., Staller, T., Germer, F., Opitz, F., Marquardt, C., Schwarz, C., Gutekunst, K., Vanselow, K.H., Schmitz, R., LaRoche, J., Schulz, R., and Appel, J.: Distribution analysis of hydrogenases in surface waters of marine and freshwater environments, PloS ONE, 5, e13846, doi:10.1371/journal.pone.0013846, 2010.

Batenburg, A. M., Walter, S., Pieterse, G., Levin, I., Schmidt, M., Jordan, A., Hammer, S., Yver, C., and Röckmann, T.: Temporal and spatial variability of the stable isotopic composition of atmospheric molecular hydrogen: observations at six EUROHYDROS stations, Atmos. Chem. Phys., 11, 6985–6999, doi:10.5194/acp-11-6985-2011, 2011.

Battino, R.: The Ostwald coefficient of gas solubility, Fluid Phase Equilib., 15, 231–240, 1984.

Bothe, H., Neuer, G., Kalbe, I., and Eisbrenner, G.: Electron donors and hydrogenase in nitrogen–fixing microorganisms, in: Stewart WDP, edited by: Gallon, J. R., Nitrogen fixation, Academic Press, London, 83–112, 1980.

Bothe, H., Schmitz, O., Yates, M. G., and Newton, W. E.: Nitrogen fixation and hydrogen metabolism in cyanobacteria, MMBR, 74, 529–51, 2010.

Breitbarth, E., Oschlies, A., and LaRoche, J.: Physiological constraints on the global distribution of *Trichodesmium* – effect of temperature on diazotrophy, Biogeosciences, 4, 53–61, 2007.

Bottinga, Y.: Calculated fractionation factors for carbon and hydrogen isotope exchange in the system calcite-carbon dioxide-graphite-methane-hydrogen-water vapour, Geochim. Cosmochim. Ac., 33, 49–64, 1969.

Chen, Q., Popa, E. M., Batenburg, A. M., and Röckmann, T.: Isotopic signatures of production and uptake of H_2 by soil, Atmos. Chem. Phys., 15, 13003–13021, doi:10.5194/acp-15-13003-2015, 2015.

Conrad, R.: Biogeochemistry and ecophysiology of atmospheric CO and H_2, Adv. Microb. Ecol., 10, 231–283, 1988.

Conrad, R. and Seiler, W.: Methane and hydrogen in seawater (Atlantic Ocean), Deep–Sea Res., 35, 1903–1917, 1988.

Constant, P., Walter, S., Batenburg, A. M., Liot, Q., and Röckmann, T.: Kinetics and isotopic signature of the H_2 uptake activity of three Actinobacteria scavenging atmospheric H_2, in preparation, 2016.

Ehhalt, D. H. and Rohrer, F.: The tropospheric cycle of H_2: a critical review, Tellus B, 61, 500–535, 2009.

Erickson, D. J. and Taylor, J. A.: 3–D Tropospheric CO modeling: The possible influence of the ocean, Geophys. Res. Lett., 19, 1955–1958, 1992

Falcón, L. I., Cipriano, F., Chistoserdov, A. Y., and Carpenter, E. J.: Diversity of diazotrophic unicellular cyanobacteria in the tropical North Atlantic Ocean, Appl. Environ. Microbiol., 68, 5760–5764, 2002.

Falcón, L. I., Carpenter, E. J., Cipriano, F., Bergman, B., and Capone, D. G.: N_2 fixation by unicellular bacterioplankton from the Atlantic and Pacific Oceans: Phylogeny and in situ rates, Appl. Environ. Microbial., 70, 765–770, 2004.

Feck, T., Grooß, J.-U., and Riese, M.: Sensitivity of Arctic ozone loss to stratospheric H_2O, Geophys. Res. Lett., 35, L01803, doi:10.1029/2007GL031334, 2008.

Feilberg, K. L., Johnson, M. S., Bacak, A., Röckmann, T., and Nielsen, C. J.: Relative tropospheric photolysis rates of HCHO and HCDO measured at the European photoreactor facility, J. Phys. Chem. A, 111, 9034–9046, 2007.

Gerst, S. and Quay, P.: Deuterium component of the global molecular hydrogen cycle, J. Geophys. Res., 106, 5021–5031, 2001.

Großkopf, T., Mohr, W., Baustian, T., Schunck, H., Gill, D., Kuypers, M. M. M., Lavik, G., Schmitz, R. A., Wallace, D .W. R., and LaRoche, J.: Doubling of marine dinitrogen–fixation rates based on direct measurements, Nature, 488, 361–364, 2012.

Hanschmann, T., Deneke, H., Roebeling, R., and Macke, A.: Evaluation of the shortwave cloud radiative effect over the ocean by use of ship and satellite observations, Atmos. Chem. Phys., 12, 12243–12253, doi:10.5194/acp-12-12243-2012, 2012.

Hauglustaine, D. A. and Ehhalt, D. H.: A three–dimensional model of molecular hydrogen in the troposphere, J. Geophys. Res., 107, 4330–4346, doi:10.1029/2001JD001156, 2002.

Herr, F. L.: Dissolved hydrogen in Eurasian Arctic waters, Tellus B, 36, 55–66, 1984.

Herr, F. L., Scranton, M. I., and Barger, W. R.: Dissolved hydrogen in the Norwegian Sea: Mesoscale surface variability and deep-water distribution, Deep–Sea Res. A, 28, 1001–1016, 1981.

Herr, F. L., Frank, E. C., Leone, G. M., and Kennicutt, M. C.: Diurnal variability of dissolved molecular hydrogen in the tropical South Atlantic Ocean, Deep–Sea Res., 31, 13–20, 1984.

Houweling, S., Dentener, F., and Lelieveld, J.: The impact of non–methane hydrocarbon compounds on tropospheric photochemistry, J. Geophys. Res, 103, 10673–10696, 1998.

Jacobson, M. Z.: Effects of wind-powered hydrogen fuel cell vehicles on stratospheric ozone and global climate, Geophys. Res. Lett., 35, L19803, doi:10.1029/2008GL035102, 2008.

Jacobson, M. Z., Colella, W. G., and Golden, D. M.: Cleaning the air and improving health with hydrogen fuel-cell vehicles, Science, 308, 1901–1905, 2005.

Jordan, A. and Steinberg, B.: Calibration of atmospheric hydrogen measurements, Atmos. Meas. Tech., 4, 509–521, 2011.

Kars, G., Gündüz, U., Yücel, M., Rakhely, G., Kovacs, K. L., and Eroğlu, İ.: Evaluation of hydrogen production by *Rhodobacter sphaeroides* O.U.001 and its *hup*SL deficient mutant using acetate and malate as carbon sources, Int. J. Hydrogen Energ., 34, 2184–2190, 2009.

Knox, M., Quay, P. D., and Wilbur, D.: Kinetic isotopic fractionation during air–water gas transfer of O_2, N_2, CH_4, and H_2, J. Geophys. Res., 97, 20335–20343, 1992.

Kock, A., Gebhardt S., and Bange, H. W.: Methane emissions from the upwelling area off Mauritania (NW Africa), Biogeosciences, 5, 1119–1125, doi:10.5194/bg-5-1119-2008, 2008.

Krol, M., Houweling, S., Bregman, B., van den Broek, M., Segers, A., van Velthoven, P., Peters, W., Dentener, F., and Bergamaschi, P.: The two-way nested global chemistry-transport zoom model

TM5: Algorithm and applications, Atmos. Chem. Phys, 5, 417–432, doi:10.5194/acp-5-417-2005, 2005.

Lilley, M. D., Baross, J. A., and Gordon, L.I.: Dissolved hydrogen and methane in Saanieh Inlet, British Columbia, Deep–Sea Res., 29, 1471–1484, 1982.

Longhurst, A. R.: Ecological Geography of the Sea, Academic, San Diego, California, 398 pp., 1998.

Moore, R. M., Punshon, S., Mahaffey, C., and Karl, D.: The relationship between dissolved hydrogen and nitrogen fixation in ocean waters, Deep–Sea Res., 56, 1449–1458, 2009.

Moore, R. M., Kienast, M., Fraser, M., Cullen, J. J., Deutsch, C., Dutkiewicz, S., Follows, M. J., and Somes, C. J.: Extensive hydrogen supersaturations in the western South Atlantic Ocean suggest substantial underestimation of nitrogen fixation, J. Geophys. Res. Oc., 119, 4340–4350, 2014.

Nilsson, E., Johnson, M. S., Taketani, F., Matsumi, Y., Hurley, M. D., and Wallington, T. J.: Atmospheric deuterium fractionation: HCHO and HCDO yields in the $CH_2DO + O_2$ reaction, Atmos. Chem. Phys., 7, 5873–5881, 2007.

Nilsson, E. J. K., Andersen, V. F., Skov, H., and Johnson, M. S.: Pressure dependence of the deuterium isotope effect in the photolysis of formaldehyde by ultraviolet light, Atmos. Chem. Phys., 10, 3455–3462, doi:10.5194/acp-10-3455-2010, 2010.

Novelli, P.C., Lang, P.M., Masarie, K.A., Hurst, D.F., Myers, R., and Elkins, J.W.: Molecular hydrogen in the troposphere: Global distribution and budget, J. Geophys. Res., 104, 30427–30444, 1999.

Pieterse, G., Krol, M. C., and Röckmann, T.: A consistent molecular hydrogen isotope chemistry scheme based on an independent bond approximation, Atmos. Chem. Phys., 9, 8503–8529, doi:10.5194/acp-9-8503-2009, 2009.

Pieterse, G., Krol, M. C., Batenburg, A. M., Steele, L. P., Krummel, P. B., Langenfelds, R. L., and Röckmann, T.: Global modelling of H_2 mixing ratios and isotopic compositions with the TM5 model, Atmos. Chem. Phys, 11, 7001–7026, doi:10.5194/acp-11-7001-2011, 2011.

Pieterse, G., Krol, M. C., Batenburg, A. M., Brenninkmeijer, C. A. M., Popa, M. E., O'Doherty, S., Grant, A., Steele, L.P., Krummel, P. B., Langenfelds, R. L., Wang, H. J., Vermeulen, A. T., Schmidt, M., Yver, C., Jordan, A., Engel, A., Fisher, R. E., Lowry, D., Nisbet, E. G., Reimann, S., Vollmer, M. K., Steinbacher, M., Hammer, S., Forster, G., Sturges, W. T., and Röckmann, T.: Reassessing the variability in atmospheric H_2 using the two-way nested TM5 model, J. Geophys. Res. Atmos, 118, 3764–3780, 2013.

Popa, M. E., Vollmer, M. K., Jordan, A., Brand, W. A., Pathirana, S. L., Rothe, M., and Röckmann, T.: Vehicle emissions of greenhouse gases and related tracers from a tunnel study: $CO:CO_2$, $N_2N_2O:CO_2$, $CH_4:CO_2$, $O_2:CO_2$ ratios, and the stable isotopes ^{13}C and ^{18}O in CO_2 and CO, Atmos. Chem. Phys., 14, 2105–2123, doi:10.5194/acp-14-2105-2014, 2014.

Popa, M. E., Segers, A. J., van der Gon, H. A. C. D., Krol, M. C., Visschedijk, A. J. H., Schaap, M., and Rockmann, T.: Impact of a future H_2 transportation on atmospheric pollution in Europe, Atmos Environ, 113, 208–222, 2015.

Prather, M. J.: An environmental experiment with H_2?, Science, 302, 581–582, 2003.

Price, H., Jaegle, L., Rice, A., Quay, P., Novelli, P. C., and Gammon, R.: Global budget of molecular hydrogen and its deuterium content: constraints from ground station, cruise, and aircraft observations, J. Geophys. Res., 112, D22108, doi:10.1029/2006JD008152, 2007.

Punshon, S. and Moore, R.: Photochemical production of molecular hydrogen in lake water and coastal seawater, Mar. Chem., 108, 215–220, 2008a.

Punshon, S. and Moore, R. M.: Aerobic hydrogen production and dinitrogen fixation in the marine cyanobacterium *Trichodesmium erythraeum* IMS101, Limnol. Oceanogr., 53, 2749–2753, 2008b.

Punshon, S., Moore, R. M., and Xie, H.: Net loss rates and distribution of molecular hydrogen (H_2) in mid-latitude coastal waters, Mar. Chem., 105, 129–139, doi:10.1016/j.marchem.2007.01.009, 2007.

Rahn, T., Kitchen, N., and Eiler, J. M.: D/H ratios of atmospheric H_2 in urban air: Results using new methods for analysis of nano-molar H_2 samples, Geochim. Cosmochim. Acta, 66, 2475–2481, 2002.

Rahn, T., Eiler, J. M., Boering, K. A., Wennberg, P. O., McCarthy, M. C., Tyler, S., Schauffler, S., Donnelly, S., and Atlas, E.: Extreme deuterium enrichment in stratospheric hydrogen and the global atmospheric budget of H_2, Nature, 424, 918–921, 2003.

Rhee, T. S., Mak, J., Röckmann, T., and Brenninkmeijer, C. A. M.: Continuous-flow isotope analysis of the deuterium/hydrogen ratio in atmospheric hydrogen, Rapid Commun. Mass Spectrom., 18, 299–306, 2004.

Rhee, T. S., Brenninkmeijer, C. A. M., and Röckmann, T.: The overwhelming role of soils in the global atmospheric hydrogen cycle, Atmos. Chem. Phys., 6, 1611–1625, doi:10.5194/acp-6-1611-2006, 2006.

Rice, A., Quay, P., Stutsman, J., Gammon, R., Price, H., and Jaegle, L.: Meridional distribution of molecular hydrogen and its deuterium content in the atmosphere, J. Geophys. Res., 115, D12306, doi:10.1029/2009JD012529, 2010.

Robinson, C., Holligan, P., Jickels, T., and Lavender, S.: The Atlantic Meridional Transect Programme (1995–2012), Deep-Sea Res.II, 56, 895–898, 2009.

Röckmann, T., Rhee, T. S., and Engel, A.: Heavy hydrogen in the stratosphere, Atmos. Chem. Phys., 3, 2015–2023, doi:10.5194/acp-3-2015-2003, 2003.

Röckmann, T., Gómez Álvarez, C. X., Walter, S., van Veen, C., Wollny, A. G., Gunthe, S. S., Helas, G., Pöschl, U., Keppler, F., Greule, M., and Brand, W. A.: The isotopic composition of H_2 from wood burning – dependency on combustion efficiency, moisture content and δD of local precipitation, J. Geophys. Res., 115, D17308, doi:10.1029/2009JD013188, 2010a.

Röckmann, T., Walter, S., Bohn, B., Wegener, R., Spahn, H., Brauers, T., Tillmann, R., Schlosser, E., Koppmann, R., and Rohrer, F.: Isotope effect in the formation of H_2 from H2CO studied at the atmospheric simulation chamber SAPHIR, Atmos. Chem. Phys., 10, 5343–5357, doi:10.5194/acp-10-5343-2010, 2010b.

Schlitzer, R.: Ocean Data View 4, http://odv.awi.de, 2012.

Schultz, M. G., Diehl, T., Brasseur, G. P., and Zittel, W.: Air pollution and climate-forcing impacts of a global hydrogen economy, Science, 302, 624–627, 2003.

Schütz, K., Happe, T., Troshina, O., Lindblad, P., Leitão, E., Oliveira, P., and Tamagnini, P.: Cyanobacterial c_{H_2} production – a comparative analysis, Planta, 218, 350–359, 2004.

Scranton, M., Jones, M., and Herr, F. L.: Distribution and variability of hydrogen in the Mediterranean Sea, J. Mar. Res., 40, 873–891, 1982.

Scranton, M. I.: The role of the cyanobacterium *Oscillatoria* (*Trichodesmium*) thiebautii in the marine hydrogen cycle, Mar. Ecol., 11, 79–87, 1983.

Seiler, W. and Schmidt, U.: Dissolved non–conservative gases in seawater, in: The sea, edited by: Goldberg, E. D., Vol 5. John Wiley & Sons, New York, 219–243, 1974.

Stal, L.J.: Is the distribution of nitrogen–fixing cyanobacteria in the oceans related to temperature?, Environ. Microbiol., 11, 1632–1645, 2009.

Tamagnini, P., Leitão, E., Oliveira, P., Ferreira, D., Pinto, F., Harris, D. J., Heidorn, T., and Lindblad, P.: Cyanobacterial hydrogenases: diversity, regulation and applications, FEMS Microbiol. Rev., 31, 692–720, 2007.

Tromp, T. K., Shia, R.-L., Allen, M., Eiler, J. M., and Yung, Y. L.: Potential environmental impact of a hydrogen economy on the stratosphere, Science, 300, 1740–1742, 2003.

Vollmer, M. K., Walter, S., Bond, S. W., Soltic, P., and Röckmann, T.: Molecular hydrogen (H_2) emissions and their isotopic signatures (H/D) from a motor vehicle: implications on atmospheric H_2, Atmos. Chem. Phys., 10, 5707–5718, doi:10.5194/acp-10-5707-2010, 2010.

Walter, S., Laukenmann, S., Stams, A. J. M., Vollmer, M. K., Gleixner, G., and Röckmann, T.: The stable isotopic signature of biologically produced molecular hydrogen (H_2), Biogeosciences, 9, 4115–4123, doi:10.5194/bg-9-4115-2012, 2012.

Walter, S., Kock, A., and Röckmann, T.: High–resolution measurements of atmospheric molecular hydrogen and its isotopic composition at the West African coast of Mauritania, Biogeosciences, 10, 3391–3403, doi:10.5194/bg-10-3391-2013, 2013.

Warwick, N. J., Bekki, S., Nisbet, E. G., and Pyle, J. A.: Impact of a hydrogen economy on the stratosphere and troposphere studied in a 2-D model, Geophys. Res. Lett., 31, L05107, doi:10.1029/2003GL019224, 2004.

Westberry, T. K. and Siegel, D. A.: Spatial and temporal distribution of *Trichodesmium* blooms in the world's oceans, Global Biogeochem. Cy., 20, GB4016, doi:10.1029/2005GB002673, 2006.

Wiesenburg, D. A. and Guinasso, N. L.: Equilibrium solubilities of methane, carbon monoxide, and hydrogen in water and sea water, J. Chem. Eng. Data, 1979, 24., 356–360, 1979.

Wilson, S. T., Foster, R. A., Zehr, J. P., and Karl, D. M.: Hydrogen production by *Trichodesmium erythraeum*, *Cyanothece* sp., and *Crocosphaera watsonii*, Aquat. Microb. Ecol., 59, 197–206, 2010a.

Wilson, S. T., Tozzi, S., Foster, R. A., Ilikchyan, I., Kolber, Z. S., Zehr, J. P., and Karl, D. M.: Hydrogen cycling by the unicellular marine diazotrophs *Crocosphaera watsonii* strain WH8501, Appl. Environ. Microb., 76, 6797–803, 2010b.

Wilson, S. T., del Valle, D. A., Robidart, J. C., Zehr, J. P., and Karl, D. M.: Dissolved hydrogen and nitrogen fixation in the oligotrophic North Pacific Subtropical Gyre, Environ. Microbiol. Rep., 5, 697–704, 2013.

Yashiro, H., Sudo, K., Yonemura, S., and Takigawa, M.: The impact of soil uptake on the global distribution of molecular hydrogen: chemical transport model simulation, Atmos. Chem. Phys., 11, 6701–6719, doi:10.5194/acp-11-6701-2011, 2011.

Yonemura, S., Kawashima, S., and Tsuruta, H.: Carbon monoxide, hydrogen, and methane uptake by soils in a temperate arable field and a forest, J. Geophys. Res., 105, 14347–14362, 2000.

Yver, C. E., Pison, I. C., Fortems-Cheiney, A., Schmidt, M., Chevallier, F., Ramonet, M., Jordan, A., Søvde, O. A., Engel, A., Fisher, R. E., Lowry, D., Nisbet, E. G., Levin, I., Hammer, S., Necki, J., Bartyzel, J., Reimann, S., Vollmer, M. K., Steinbacher, M., Aalto, T., Maione, M., Arduini, J., O'Doherty, S., Grant, A., Sturges, W. T., Forster, G. L., Lunder, C. R., Privalov, V., Paramonova, N., Werner, A., and Bousquet, P.: A new estimation of the recent tropospheric molecular hydrogen budget using atmospheric observations and variational inversion, Atmos. Chem. Phys., 11, 3375–3392, doi:10.5194/acp-11-3375-2011, 2011.

Zehr, J. P., Waterbury, J. B., Turner, P. J., Montoya, J. P., Omoregie, E., Steward, G. F., Hansen, A., and Karl, D. M.: Unicellular cyanobacteria fix N_2 in the subtropical North Pacific Ocean, Nature, 412, 635–638, 2001.